Development of a cloud framework for training and deployment of deep learning models in Radiology: automatic segmentation of the human spine from CT-scans as a case-study

Rui Santos[1]*, Nicholas Bünger[1]*, Benedikt Herzog[1],, and Sebastiano Caprara[1#]

[1]Digital Medicine Unit, Balgrist University Hospital Zürich, University of Zürich, Forchstrasse 340, 8008, Zurich, CH, Switzerland.
*Equally contributing authors
[#]Corresponding author: sebastiano.caprara@balgrist.ch

Abstract

Advancements in artificial intelligence (AI) and the digitalization of healthcare are revolutionizing clinical practices, with the deployment of AI models playing a crucial role in enhancing diagnostic accuracy and treatment outcomes. Our current study aims at bridging image data collected in a clinical setting, with deployment of deep learning algorithms for the segmentation of the human spine. The developed pipeline takes a decentralized approach, where selected clinical images are sent to a trusted research environment, part of private tenant in a cloud service provider. As a use-case scenario, we used the TotalSegmentator CT-scan dataset, along with its annotated ground-truth spine data, to train a ResSegNet model native to the MONAI-Label framework. Training and validation were conducted using high performance GPUs available on demand in the Trusted Research Environment. Segmentation model performance benchmarking involved metrics such as dice score, intersection over union, accuracy, precision, sensitivity, specificity, bounding F1 score, Cohen's kappa, area under the curve, and Hausdorff distance. To further assess model robustness, we also trained a state-of-the-art nnU-Net model using the same dataset and compared both models with a pre-trained spine segmentation model available within MONAI-Label. The ResSegNet model, deployable via MONAI-Label, demonstrated performance comparable to the state-of-the-art nnU-Net framework, with both models showing strong results across multiple segmentation metrics. This study successfully trained, evaluated and deployed a decentralized deep learning model for CT-scan spine segmentation in a cloud environment. This new model was validated against state-of-the-art alternatives. This comprehensive comparison highlights the value of the MONAI-Label as an effective tool for label generation, model training, and deployment, further highlighting its user-friendly nature and ease of deployment in clinical and research settings. Further we also demonstrate that such tools can be deployed in private and safe decentralized cloud environments for clinical use.

Key words: U-Net, ResSegNet, nnU-Net, deep-learning, framework, MONAI, cloud computing

Abbreviations:

DL: deep learning; AI: artificial intelligence; AUC: area under the curve

Author Summary:

In the rapidly evolving field of medical imaging, the integration of artificial intelligence (AI) and cloud computing is becoming increasingly critical for advancing diagnostic and treatment capabilities. To address the growing demand for flexible digital frameworks in the clinical environment supporting the deployment of data-driven applications, we have developed and deployed a cloud-based Trusted Research Environment designed specifically for training, validation, and deployment of deep learning models focused on semantic segmentation in musculoskeletal radiology. This environment facilitates the efficient handling of large datasets and the accessibility of algorithmic output for the physicians, optimizing the interface between development and clinical translation. The established framework enables significant improvements in the deployment of deep learning tools for image analysis in the clinical setting. In our current use-case, we have utilized this environment to train and evaluate two advanced deep learning models for the segmentation of the human spine from CT scans. By leveraging the computational power and flexibility of the cloud-based infrastructure, we were able to perform rigorous training and comparison of these models, aiming to enhance the accuracy and reliability of spine segmentation in clinical practice. This approach not only streamlines the process of model development but also provides valuable insights into the performance and potential clinical applications of these AI-driven segmentation tools.

Introduction

With the inflection point of Artificial Intelligence (AI) algorithms, with its deep learning (DL) models and frameworks (1), medical operations are facing the paradigm shift of both digitalization and DL models deployment. Out of all clinical specialties, Radiology is poised to be at the forefront of this transformation due to its inherent reliance on visual data and the well-established role of image analysis in diagnosis and treatment planning (2,3). As such, there is a strong research focus on developing and deploying AI models within the Radiology field. As an example, in the past 5 years (2019-2023), a total of 11'392 research manuscripts (PubMed search) were related in some form with the thematic of radiology and deep learning (DL). Indeed, medical imaging is a key area for the development of high added-value DL models that streamline and accelerate the process of image segmentation and classification, which is a major time-consuming task for physicians (4).

Several AI tools have been developed with the objective of accelerating medical image segmentation. Recently, the development of the TotalSegmentator DL model (5), trained to segment 117 anatomical structures (version 2.0), from CT datasets, demonstrates the immense

possibilities that DL-powered medical image segmentation offers. For the development of such a powerful DL segmentation model, the nnU-Net framework was used (6). This framework allows the training of state-of-the art segmentations models, based on the U-Net DL architecture (7), with minimal to no coding needed. Still, these tools are limited in their deployment in daily clinical scenarios. As an easier and user-oriented approach, the open-source framework MONAI (Medical Open Network for Artificial Intelligence) (8) has been developed for the training and easier deployment of automatic medical image segmentation models. At the forefront of MONAI, the sub-framework MONAI-Label (9) connects DL architectures and pretrained models with open-source graphic user interfaces (GUI) such as 3D Slicer and OHIF (Open Health Imaging Foundation Viewer), enabling active learning with direct visualization and correction of segmentation results (10,11).

As optimal environment for the deployment of such aforementioned frameworks, the adoption of cloud computing in medical research setting, offers many benefits: it fosters improved collaboration among physicians and researchers, provides a decentralized and scalable computing infrastructure and greater accessibility to tools and services such as giving support for data annotation. Furthermore, cloud-based infrastructure offers simplified management of resources in a cost-effective manner, allowing medical research centers to focus resources on data analysis and clinical relevance of research questions rather than IT maintenance (12,13).

In this study, we have developed a cloud computing framework leveraging the open-source pipeline of MONAI-Label for the development and deployment for clinical research teams of an interactive spine segmentation model out of CT data. Moreover, we benchmarked the model output with an in-house trained nnU-Net model, both trained and validated with the same collection of images (TotalSegmentator open-source dataset). We also compare it with a pretrained model for spine segmentation present in MONAI-Label, trained on the VERSE dataset (14). We demonstrate that the MONAI-Label developed model produces similar segmentation results to the model trained with the nnU-Net framework yet providing a far simpler vertical integration in a clinical research setting. This *de novo* trained model also considerably outperforms the pretrained spine segmentation model present in MONAI-Label *ab initio*. Moreover, the presented research highlights the use of MONAI-Label as a powerful tool for developing DL models and automatically generating anatomical segmentation of anatomical structures which may support surgical planning, diagnostics and future creation of digital twins of patients (15,16).

Materials and Methods

Architecture of a trusted cloud research environment for deep learning model training and deployment

The framework introduced in this work is based on a private cloud environment composed of private endpoints, i.e., a pointer to the location of the data, which allows the hospital network to be extended in a private cloud space (figure 1A). Through an Application Programming Interface (API) Manager, the DICOM (Digital Imaging and Communications in Medicine standard) or NIFTI (Neuroimaging Informatics Technology Initiative) storage locations connect with cloud computational nodes (with adequate hardware accelerators, such as graphic processing units – GPUs), and a centralized management dashboard that allows the definition of strict governance policies, as the ones in place at healthcare institutions, granting secure and private access to specified users. Through the combination of the cloud services mentioned above, the framework composed of 3D Slicer and MONAI Label-based computational nodes was developed. In this way, scalable computation resources are connected with a Graphical User Interface (GUI) thanks to the open-source tool 3D Slicer, as shown on figure 1b.

For segmentation model training in the trusted research environment, the TotalSegmentator open-source image dataset was stored in a project-specific NIFTI storage and connected with computational resources embedded in the computational node via the API Manager.

For segmentation inference, an additional API allows the access to DICOM images stored in the clinical PACS (Picture Archiving and Communication System), retrieve these images to a DICOM storage location in the cloud which then directly connects to the MONAI Label computational node for automatic segmentation processing. The connection to the GUI results in a user-friendly environment where radiologists and other physicians can visualize the segmentation results, correct them, and potentially fine-tuning the models by sending the corrected results back to MONAI Label central instance to update the training.

Resources for deep learning model training

The TotalSegmentator dataset composed of CT images and their ground-truth vertebrae and sacrum segmentations (part of the open-source dataset) was used for model training in either the MONAI-Label or nnU-Net frameworks (5) (https://zenodo.org/records/10047292, with an average isotropic pixel size of 1.5 mm). The dataset was divided into training and inference dataset. 964 images were randomly chosen to be part of the training dataset, while the remaining 108 were used for validation (the open-source version of the dataset contains more than 1200 images, nonetheless, some cannot be used with the current version, 2.0.1). The dataset was preprocessed in accordance with the requirements of both MONAI-Label and nnU-Net

(instructions found at https://github.com/Project-MONAI/MONAILabel?tab=readme-ov-file#getting-started-with-monai-label and https://github.com/MIC-DKFZ/nnUNet). The dataset was uploaded into a storage location in the developed cloud-based Trusted Research Environment. The default segmentation task in MONAI-Label , based on a ResSegNet architecture (17), was used for spine segmentation model training. The training was performed in 4 A100 GPU computational nodes, for 1000 epochs, 241 iterations each, taking *circa* 25 hours of compute time. Since for both training and results analysis a graphic user interface is necessary, the open-source 3D Slicer tool was used in a container (https://github.com/pieper/SlicerDockers, v5.0.3). No validation split was used in this training as model benchmarking would be done with an already assigned dataset (remaining 108 images available). Default segmentation pipeline scripts were used with no modifications (segmentation.py, part of the radiology app from the MONAI-Label framework with a tutorial found here: https://github.com/Project-MONAI/tutorials/tree/main/monailabel). The nnU-Net model training was performed on one A100 compute node for 1000 epochs, 250 iterations each, over the course of 15 hours of training. No validation split was used (fold 0), as model benchmarking would be done with an already assigned dataset (same 108 datasets used to validate the MONAI-Label model). Default nnU-Net pipeline scripts were used with no modifications, following the developers tutorial.

Deep learning model benchmarking

108 CT scans of the TotalSegmentator dataset (not part of the dataset for DL model training) were used for model validation. We calculated different segmentation metrics to benchmark both deep learning models' segmentation results such as dice score, intersection over union, accuracy, precision, sensitivity, specificity, bounding F1 score, recall, area under the curve (AUC) and the Hausdorff distance between segmentation predictions and their ground truth (18). Each metric was calculated with custom scripts (available upon request). Calculation of distances between ground truth and predicted segmentations was done in the open-source software Meshlab (https://www.meshlab.net/) v2022.02 with built-in functions. P-values were calculated based on a non-paired t-student function.

Results

Benefits of a decentralized cloud infrastructure for DL model training and deployment

Deploying a decentralized trusted research environment on the cloud for training and deployment of deep learning models present two major benefits: on one hand the scalability and flexibility to

compose a tailored DL model for a specific research or clinical question, on the other hand, the possibility to deploy the developed models in clinical workflows using the same architecture.
Depending on the size and architecture of the model, the compute resources of the computational nodes can be quickly scaled-up or scaled-down, providing the creation of an optimized setup for each use-case requiring a training, validation and/or deployment of a research or clinical DL model. Further, this decentralized approach makes it far simpler to securely and privately connect different medical devices (CT scanners, MRI machines, ultrasound machines, etc.) as endpoints to the developed trusted research environment and get outputs in real-time.
Within the MONAI Label framework, multiple models can easily be retrieved and fine-tuned by labeling additional data via a user-friendly GUI, in this way a local version can be trained. The versatility of this process enables various healthcare operators, e.g. radiologists, to retrain models on top of open-source available models (transfer learning). Furthermore, they can easily test models that have been previously created in the framework and validate them thanks to commonly available software for 3D visualization. This way, the interaction between model's development and radiologists is considerably improved and physicians are a central component in the development of new ML models.

Training a ResSegNet based CT-scan spine segmentation model within the MONAI-Label framework: spineCT-ResSegNet model

Out of 1072 images present in the TotalSegmentator, 964 images (90% of the dataset), were randomly chosen to compose the training dataset, while 108 (remaining dataset) served as the validation dataset. Default 3D ResSegNet parameters of the segmentation (ResSegNet) task of MONAI-Label radiology app, were used. Qualitative analysis of the segmentation results (figure 2A) demonstrates the capacity of robust prediction of the entire human spine and sacrum (25 segmented classes). Vertebral bodies identification is correctly done, with their shape being in accordance with anatomical expectancy. Quantitative segmentation quality metrics over all the 25 classes reveal a robust model for spine segmentation from CT-scans with an average dice score of 0.856±0.066, an average intersection over union score of 0.801±0.074, average accuracy of 1.000±0.000, a mean precision of 0.862±0.066, a mean sensitivity (or recall) of 0.861±0.070, a mean specificity of 1.000±0.000, an average bounding F1 score of 0.837±0.057, a mean area under the curve (AUC) of 0.932±0.034 and a Kappa of 0.853±0.068 (figure 2B, all numbers rounded to 3 decimal places). Detailed results, with 95% confidence intervals, are found in supplementary figure 1.

Training a nnU-Net based CT-scan spine segmentation model: spineCT-nnUNet model

Serving as a benchmark for DL segmentation model comparison, we trained the nnU-Net framework on the same dataset [OBJ], with the 3D-UNet full resolution model (1.5 mm), using the default configuration and trained the model over 1000 epochs. Validation was performed with the same 108 CT scans as for the MONAI-Label ResSegNet model, native to MONAI-Label. Segmentation output is qualitatively robust with anatomical structures, i.e. vertebrae, are localized to their correct position and have a correct tridimensional conformational (figure 3A). [OBJ]between the segmentation prediction and their ground-truth, reveal a robust prediction model, with an average dice score over the 25 classes (anatomical structures) of 0.914±0.036, an average intersection over union of 0.879±0.045, an accuracy of 1.000±0.000, a precision of 0.911±0.046, a sensitivity (or recall) of 0.910±0.050, a specificity of 1.000±0.000, a boundary F1 score of 0.908±0.029, an AUC score of 0.961±0.018 and a Kappa score of 0.904±0.049 (figure 3B, 5 all numbers rounded to 3 decimal places). Detailed results, with 95% confidence intervals, are found in supplementary figure 2.

Comparison of spineCT-ResSegNet, spineCT-nnUNet and pretrained spine segmentation models

To further compare the segmentation predictions between the ResSegNet model and the nnU-Net model to the respective ground truth, we overlaid selected examples as exemplified in figure 4A (spineCT-ResSegNet) and 4C (spineCT-nnUNet). Hausdorff distances between each segmentation model predictions and their ground truths were calculated (spineCT-ResSegNet and spineCT-nnUNet in figure 4B and figure 4D respectively). The spineCT-ResSegNet model presents an average Hausdorff distance of 2.604±0.450 mm while the spineCT-nnUNet model predictions present a Hausdorff distance of 2.214±0.398. While the nnU-Net based model outperforms the ResSegNet model in regard to the quality metric of Hausdorff distance, the same is not observed for the remaining metrics calculated. Thus, we find sufficient evidence to say both models produce on-par segmentation results (supplementary figure 5A, all p-valued rounded to 5 decimal plates).

We also benchmarked the pretrained vertebrae segmentation model which is part of the MONAI-Label core. The model spine segmentation predictions average a dice score over the 24 classes (as this model only predicts from C1 to L5) of 0.601±0.153, an average intersection over union of 0.533±0.154, an accuracy of 1.000±0.000, a precision of 0.697±0.150, a sensitivity (or recall) of 0.565±0.157, a specificity of 1.000±0.000, a boundary F1 score of 0.588±0.144, an AUC score of 0.785±0.080 and a Kappa score of 0.597±0.151 (supplementary figure 3, all numbers rounded

to 3 decimal places). The output segmentations present a Hausdorff distance of 3.129±0.322 mm on average. Thus, we can demonstrate that the *de novo* trained model spineCT-ResSegNet outperforms the pretrained model in MONAI-Label in most quality metrics calculated (supplementary figure 5B, all p-valued rounded to 5 decimal plates). Furthermore, it also trained in one more class, the sacrum.

Discussion

A decentralized trusted research environment as a core of novel digital ecosystems in medical research has the potential to simplify communication between physicians and researchers, enable effective testing and validation of novel tools, provide secure and private data exchange channels - and ultimately reduce costs by sharing computational resources, with non-complicated scalability. Further benefits are the ability to access common datasets, shared code, and validation methods at any time reduces errors and improves usability - and thus accelerates the clinical translation of digital technologies. Altogether, such platforms facilitate testing and validation of digital and DL pipelines, making data-driven medical research more reproducible and better suited for the deployment in clinical settings. With these principles in mind, we developed a radiology-specific cloud infrastructure, based on a combination of DICOM storage services and MONAI-Label-compatible computational nodes for the training and deployment of deep learning segmentation models.

As a case-study, we trained and deployed a ResSegNet model for human spine segmentation out the open-source dataset of CT-scans from TotalSegmentator. This model was trained as part of the MONAI-Label (8,19) framework. As a benchmark, we used the nnU-Net framework (6) and also trained a segmentation model with the same training and inference dataset. Both models yielded similar quality metric results with only average Hausdorff distance being noticeable better for the nnU-Net model, than for the ResSegNet model (figure 4 and supplementary figure 5). Nonetheless, given the native deployment of the ResSegNet model via MONAI-Label, we can directly deploy it via a graphic user interface such as 3D Slicer or OHIF (10,11), which is not possible with the nnU-Net, at least not in a straightforward way. This in-place visualization provides direct access to the segmentation results to the health professionals who can use it to make informed decisions, e.g. for surgical planning.

We also compared our trained model, spineCT-ResSegNet, with the pre-trained and pre-built spine segmentation model which MONAI-Label already offers (14). Our newly trailed model greatly outperforms the prebuilt model in all metrics, providing substantially more accurate segmentations (supplemental figure 4 and 5).

While our developed models underperformed compared with the dice scores reported for the TotalSegmentator model (average 0.95 for vertebrae) (5), this nnU-Net based model was trained for 8000 epochs compared to ours which was trained for only 1000 epochs. This meant a far lower training time for our model, fewer computational resources were needed, while still performing adequately for the task at hand.

Naturally, given the dice coefficient of around 0.85 and a hausdorff coefficient of approximately 2.6 mm, the ResSegNet model incurs in mispredictions and proper segmentation correction may be necessary. Nonetheless, the iterative nature and easy of use of MONAI-Label and a chosen GUI such as 3d Slicer, makes any necessary corrections easy to perform. Further, this corrections may be included as part of a subsequent finetuned model, as part of the labelling correction process, which will then, increase the predictive power of the model.

Conclusion

The present research demonstrates the potential of cloud-based deep learning for training and deployment of medical image segmentation models, in a trusted research environment. By leveraging the efficiency and scalability of cloud computing, we have created a framework that empowers medical professionals, such as radiologists, with faster, more accessible segmentation tools, based on the MONAI-Label open-source framework. This paves the way for improved diagnostics, treatment planning, and ultimately, better patient outcomes.

Author Contribution

NB developed and deployed the trusted cloud environment. RS worked on the development and testing of the deep learning segmentation models. BH assisted NB in the infrastructure setting of the trusted cloud environment. NB, RS and SC wrote the manuscript and designed the figures. SC supervised the design of the infrastructure and pipeline and contributed to the design of the research and interpretation of the results. MF contributed to the final version of the manuscript.

Acknowledgements

The authors acknowledge the Digital Society Initiative, University of Zurich. This work is part of the DSI-Infrastructure / Lab-Program.

References

1. Sevilla J, Heim L, Ho A, Besiroglu T, Hobbhahn M, Villalobos P. Compute Trends Across Three Eras of Machine Learning. Proceedings of the International Joint Conference on Neural Networks. Institute of Electrical and Electronics Engineers Inc.; 2022. doi: 10.1109/IJCNN55064.2022.9891914.

2. Saba L, Biswas M, Kuppili V, et al. The present and future of deep learning in radiology. Eur J Radiol. Elsevier Ireland Ltd; 2019. p. 14–24. doi: 10.1016/j.ejrad.2019.02.038.

3. Chea P, Mandell JC. Current applications and future directions of deep learning in musculoskeletal radiology. Skeletal Radiol. Springer; 2020. p. 183–197. doi: 10.1007/s00256-019-03284-z.

4. Langlotz CP. The Future of AI and Informatics in Radiology: 10 Predictions. Radiology. Radiological Society of North America Inc.; 2023. doi: 10.1148/radiol.231114.

5. Wasserthal J, Breit HC, Meyer MT, et al. TotalSegmentator: Robust Segmentation of 104 Anatomic Structures in CT Images. Radiol Artif Intell. Radiological Society of North America Inc.; 2023;5(5). doi: 10.1148/RYAI.230024/ASSET/IMAGES/LARGE/RYAI.230024.VA.JPEG.

6. Isensee F, Jaeger PF, Kohl SAA, Petersen J, Maier-Hein KH. nnU-Net: a self-configuring method for deep learning-based biomedical image segmentation. Nature Methods 2020 18:2. Nature Publishing Group; 2020;18(2):203–211. doi: 10.1038/s41592-020-01008-z.

7. Ronneberger O, Fischer P, Brox T. U-net: Convolutional networks for biomedical image segmentation. Lecture Notes in Computer Science (including subseries Lecture Notes in Artificial Intelligence and Lecture Notes in Bioinformatics). Springer Verlag; 2015. p. 234–241. doi: 10.1007/978-3-319-24574-4_28.

8. Jorge Cardoso M, Li W, Brown R, et al. MONAI: An open-source framework for deep learning in healthcare. 2022;

9. Diaz-Pinto A, Alle S, Nath V, et al. MONAI Label: A framework for AI-assisted Interactive Labeling of 3D Medical Images. 2022; doi: 10.1016/j.media.2024.103207.

10. Fedorov A, Beichel R, Kalpathy-Cramer J, et al. 3D Slicer as an image computing platform for the Quantitative Imaging Network. Magn Reson Imaging. 2012;30(9):1323–1341. doi: 10.1016/j.mri.2012.05.001.

11. Ziegler E, Urban T, Brown D, et al. Open Health Imaging Foundation Viewer: An Extensible Open-Source Framework for Building Web-Based Imaging Applications to Support Cancer Research. JCO Clin Cancer Inform. 2020. https://doi.org/10.

12. Griebel L, Prokosch HU, Köpcke F, et al. A scoping review of cloud computing in healthcare. BMC Med Inform Decis Mak. BioMed Central Ltd; 2015. doi: 10.1186/s12911-015-0145-7.

13. Navale V, Bourne PE. Cloud computing applications for biomedical science: A perspective. PLoS Comput Biol. Public Library of Science; 2018;14(6). doi: 10.1371/journal.pcbi.1006144.

14. Sekuboyina A, Husseini ME, Bayat A, et al. VERSE: A Vertebrae labelling and segmentation benchmark for multi-detector CT images. Med Image Anal. Elsevier B.V.; 2021. doi: 10.1016/j.media.2021.102166.

15. Caprara S, Carrillo F, Snedeker JG, Farshad M, Senteler M. Automated Pipeline to Generate Anatomically Accurate Patient-Specific Biomechanical Models of Healthy and Pathological FSUs. Front Bioeng Biotechnol. Frontiers Media S.A.; 2021;9. doi: 10.3389/fbioe.2021.636953.

16. Iqbal JD, Krauthammer M, Biller-Andorno N. The Use and Ethics of Digital Twins in Medicine. Journal of Law, Medicine and Ethics. Cambridge University Press; 2022;50(3):583–596. doi: 10.1017/jme.2022.97.

17. Saxena N, Babu NK, Raman B. Semantic segmentation of multispectral images using res-seg-net model. Proceedings - 14th IEEE International Conference on Semantic Computing, ICSC 2020. Institute of Electrical and Electronics Engineers Inc.; 2020. p. 154–157. doi: 10.1109/ICSC.2020.00030.

18. Müller D, Soto-Rey I, Kramer F. Towards a guideline for evaluation metrics in medical image segmentation. BMC Res Notes. BioMed Central Ltd; 2022. doi: 10.1186/s13104-022-06096-y.

19. Diaz-Pinto A, Alle S, Nath V, et al. MONAI Label: A framework for AI-assisted Interactive Labeling of 3D Medical Images. 2022; http://arxiv.org/abs/2203.12362.

Figure Legends

Figure 1: Architecture of the cloud infrastructure behind the trusted research environment and deployed framework with 3D Slicer and MONAI-Label. (A) Overview of the components of the architecture of the trusted research environment: storage and compute. The first one has a DICOM blob storage which is exposed with a private endpoint; while the second one has more components. The compute workspace is exposed as well with a private endpoint, while the other component such as storage account, key vault Jupyter notebook and container registry are connected to the workspace. Both systems have group permissions that can be managed individually. To access the trusted research environment, users can use a Virtual Desktop application **(B)** Using two compute nodes, 3D Slicer and MONAI Label are deployed separately. With an SSH connection users can access an online environment to use the 3D Slicer interface to interact with the model's output that runs on the first compute node (from the left side), which process the DICOM images retrieved by the second compute node on which MONAI Label is running from the DICOM blob storage.

Figure 2 – SpineCT-ResSegNet spine segmentation model predictions and segmentation metrics. (A) Example of segmentation results with the spineCT-ResSegNet, a trained MONAI-Label native model, in both 2D and 3D visualizations. Vertebrae are color coded. The entire human spine is represented in the image: cervical spine (C1-C7), thoracic spine (T1-T12), Lumbar spine (L1-L5) and sacrum. (B) Validation metrics for spineCT-ResSegNet spine segmentation model, based on the prediction of 108 cases. Color encodes the accuracy of segmentation class predictions. Blue indicates high similarity to the ground truth, while red represents increasing deviation from the actual values.

Figure 3 – SpineCT-nnUNet spine segmentation model predictions and segmentation metrics. (A) Example of segmentation results with the nnU-Net framework derived model (3D-full resolution) in both 2D and 3D visualizations. Vertebrae are color coded. The entire human spine is represented in the image: cervical spine (C1-C7), thoracic spine (T1-T12), Lumbar spine (L1-L5) and sacrum. (B) Validation metrics for spineCT-nnUNet spine segmentation model. Color encodes the accuracy of segmentation class predictions. Blue indicates high similarity to the ground truth, while red represents increasing deviation from the actual values.

Figure 4 – Comparison of spineCT-ResSegNet and spineCT-nnUNet semantic segmentation models. (A) Example of the Hausdorff distance calculation between the spineCT-ResSegNet model (native to MONAI-Label) predictions and ground truth. (B) Average Hausdorff distance calculation for spineCT-ResSegNet predictions versus their ground truth. Predictions with the spineCT-ResSegNet model average a Hausdorff Distance of 2.604±0.450 mm to the ground truth. (C) Example of the Hausdorff distance calculation between the spineCT-nnUNet model predictions and ground truth. (D) Average Hausdorff distance calculation for spineCT-nnUNet predictions versus their ground truth. Predictions with the spineCT-nnUNet model average a Hausdorff Distance of 2.214±0.398 mm to the ground truth. Color encoding in (B) and (D) correlates with the accuracy of segmentation class predictions. Blue indicates high similarity to the ground truth, while red represents increasing deviation from the actual values.

Supplemental Figure 1 – Comprehensive metrics evaluation of the spineCT-ResSegNet. Average metrics for the spineCT-ResSegNet model based on comparison between the predictions of the model on 108 datasets and their ground truth.

Supplemental Figure 2 – Comprehensive metrics evaluation of the spineCT-nnUNet. Average metrics for the spineCT-ResSegNet model based on comparison between the predictions of the model on 108 datasets and their ground truth.

Supplemental Figure 3 – Comprehensive metrics evaluation of the open-source vertebrae segmentation model of MONAI-Label. Average metrics for the spineCT-ResSegNet model based on comparison between the predictions of the model on 108 datasets and their ground truth.

Supplementary Figure 4 – Hausdorff distance between prediction and ground truth by the open-source vertebrae segmentation model of MONAI-Label. (A) Example of the Hausdorff distance calculation between the spineCT-ResSegNet model (native to MONAI-Label) predictions and ground truth. (B) The pre-trained model present in MONAI-Label, trained on the VERSE dataset averages a Hausdorff Distance of 3.129±0.322 mm between model segmentation prediction and ground truth.

Supplementary Figure 5 – Statistical significance analysis between the quality segmentation metrics for each method used. (A) On average, both models, spineCT-

ResSegNet and spineCT-nnUNet outputs are similar with the later one outperforming the MONAI-Label native model, only in regard to Hausdorff distance. Thus, both models appear to have a relatively equal prediction quality. (B) The newly trained spineCT-ResSegNet model mostly outperforms the pre-built spine segmentation model present in the MONAI-Label framework. Further, the model was trained in one extra class, the sacrum, capable of performing robust predictions for the anatomical class.

Figure 1

A

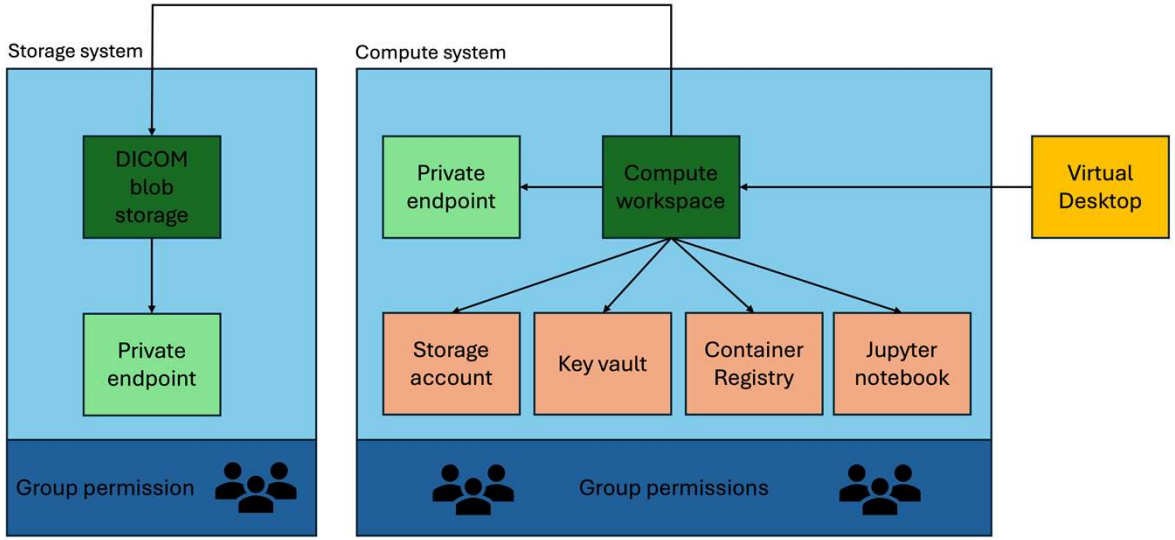
Storage system
Compute system
DICOM blob storage
Private endpoint
Private endpoint
Compute workspace
Virtual Desktop
Storage account
Key vault
Container Registry
Jupyter notebook
Group permission
Group permissions

B

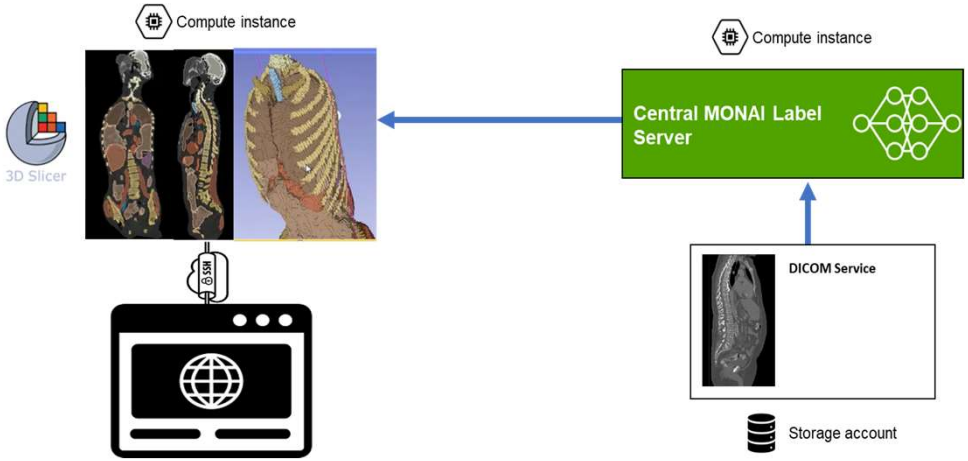
Compute instance
Compute instance
3D Slicer
Central MONAI Label Server
DICOM Service
Storage account

Figure 2

A

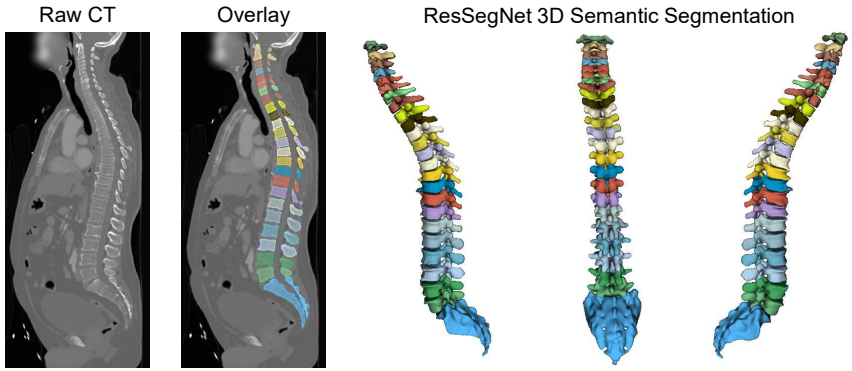

B

Metric	DICE Score		IoU		Accuracy		Precision		Sensitivity		Specificity		Boundary F1 Score		AUC		Kappa	
Class	Average	SD	Average	SD	Average	SD	Average	SD	Average	SD	Average	SD	Average	SD	Average	SD	Average	SD
C1	0.807	0.330	0.758	0.314	1.000	0.000	0.796	0.327	0.820	0.336	1.000	0.000	0.792	0.325	0.910	0.168	0.806	0.330
C2	0.891	0.219	0.846	0.226	1.000	0.000	0.877	0.233	0.915	0.212	1.000	0.000	0.880	0.212	0.957	0.106	0.891	0.219
C3	0.891	0.211	0.840	0.207	1.000	0.000	0.907	0.204	0.877	0.213	1.000	0.000	0.894	0.134	0.939	0.107	0.890	0.211
C4	0.896	0.110	0.826	0.155	1.000	0.000	0.895	0.145	0.911	0.090	1.000	0.000	0.890	0.107	0.955	0.045	0.896	0.110
C5	0.647	0.405	0.589	0.382	1.000	0.000	0.668	0.423	0.655	0.397	1.000	0.000	0.654	0.399	0.827	0.198	0.647	0.405
C6	0.737	0.311	0.656	0.306	1.000	0.000	0.762	0.324	0.725	0.343	1.000	0.000	0.734	0.296	0.872	0.165	0.723	0.324
C7	0.812	0.222	0.724	0.225	1.000	0.000	0.874	0.204	0.792	0.219	1.000	0.000	0.783	0.196	0.896	0.110	0.812	0.222
T1	0.883	0.159	0.814	0.172	1.000	0.000	0.839	0.166	0.945	0.146	1.000	0.000	0.846	0.134	0.973	0.073	0.883	0.159
T2	0.892	0.215	0.846	0.221	1.000	0.001	0.905	0.212	0.882	0.218	1.000	0.000	0.883	0.183	0.941	0.109	0.892	0.215
T3	0.811	0.277	0.748	0.289	1.000	0.000	0.840	0.268	0.783	0.309	1.000	0.000	0.815	0.237	0.899	0.147	0.799	0.292
T4	0.804	0.282	0.739	0.295	1.000	0.001	0.775	0.289	0.850	0.268	1.000	0.000	0.787	0.251	0.925	0.134	0.803	0.282
T5	0.830	0.267	0.771	0.279	1.000	0.001	0.838	0.267	0.826	0.270	1.000	0.001	0.823	0.230	0.913	0.135	0.830	0.267
T6	0.782	0.311	0.722	0.319	1.000	0.001	0.783	0.310	0.786	0.313	1.000	0.000	0.780	0.269	0.893	0.157	0.782	0.312
T7	0.816	0.259	0.748	0.280	1.000	0.001	0.798	0.293	0.813	0.298	1.000	0.000	0.805	0.224	0.920	0.133	0.793	0.289
T8	0.879	0.195	0.819	0.214	1.000	0.001	0.858	0.234	0.888	0.207	1.000	0.000	0.850	0.173	0.951	0.089	0.866	0.219
T9	0.878	0.229	0.830	0.241	1.000	0.001	0.883	0.237	0.877	0.221	1.000	0.001	0.853	0.202	0.938	0.111	0.878	0.229
T10	0.894	0.223	0.855	0.237	1.000	0.001	0.911	0.217	0.882	0.231	1.000	0.001	0.877	0.195	0.941	0.116	0.894	0.223
T11	0.917	0.171	0.877	0.194	1.000	0.001	0.915	0.169	0.923	0.175	1.000	0.000	0.895	0.147	0.961	0.088	0.917	0.172
T12	0.915	0.166	0.872	0.190	1.000	0.001	0.909	0.195	0.909	0.194	1.000	0.000	0.885	0.152	0.961	0.081	0.903	0.195
L1	0.900	0.198	0.856	0.220	1.000	0.001	0.917	0.197	0.906	0.175	1.000	0.000	0.870	0.191	0.953	0.087	0.900	0.198
L2	0.870	0.211	0.815	0.247	1.000	0.001	0.920	0.189	0.864	0.189	1.000	0.000	0.851	0.181	0.932	0.095	0.870	0.211
L3	0.904	0.162	0.853	0.197	1.000	0.002	0.912	0.172	0.912	0.154	1.000	0.001	0.869	0.150	0.956	0.077	0.904	0.163
L4	0.883	0.211	0.833	0.230	1.000	0.001	0.908	0.218	0.889	0.177	1.000	0.001	0.846	0.188	0.944	0.088	0.883	0.211
L5	0.914	0.134	0.859	0.154	1.000	0.001	0.906	0.103	0.936	0.137	1.000	0.000	0.867	0.130	0.968	0.068	0.914	0.134
Sacrum	0.956	0.033	0.917	0.055	1.000	0.000	0.965	0.044	0.949	0.039	1.000	0.000	0.905	0.044	0.975	0.020	0.956	0.033
Average	0.856		0.801		1.000		0.862		0.861		1.000		0.837		0.932		0.853	
SD	0.066		0.074		0.000		0.066		0.070		0.000		0.057		0.034		0.068	

Figure 3

A

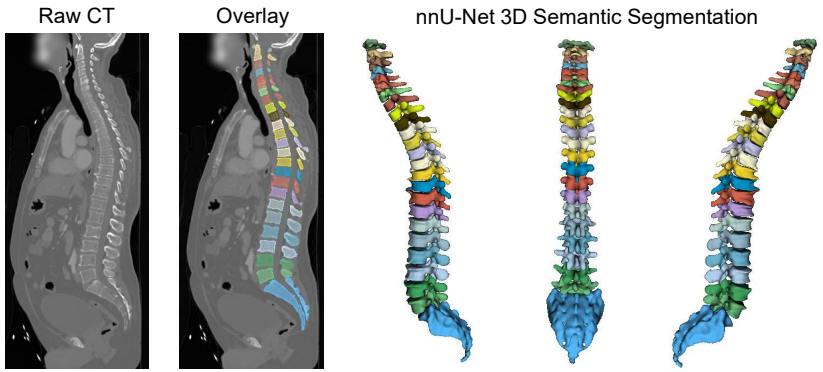

B

Metric	DICE Score		IoU		Accuracy		Precision		Sensitivity (recall)		Specificity		Boundary F1 Score		AUC		Kappa	
Class	Average	SD	Average	SD	Average	SD	Average	SD	Average	SD	Average	SD	Average	SD	Average	SD	Average	SD
C1	0.843	0.303	0.805	0.308	1.000	0.000	0.847	0.337	0.790	0.353	1.000	0.000	0.838	0.296	0.917	0.155	0.806	0.345
C2	0.911	0.220	0.880	0.227	1.000	0.000	0.901	0.230	0.928	0.213	1.000	0.000	0.908	0.213	0.964	0.107	0.911	0.220
C3	0.936	0.086	0.890	0.123	1.000	0.000	0.970	0.025	0.914	0.122	1.000	0.000	0.943	0.033	0.957	0.061	0.936	0.086
C4	0.901	0.170	0.848	0.203	1.000	0.000	0.940	0.105	0.900	0.192	1.000	0.000	0.915	0.103	0.950	0.096	0.901	0.170
C5	0.794	0.271	0.720	0.287	1.000	0.000	0.795	0.336	0.750	0.332	1.000	0.000	0.822	0.250	0.904	0.138	0.747	0.324
C6	0.909	0.086	0.843	0.128	1.000	0.000	0.791	0.296	0.852	0.299	1.000	0.000	0.911	0.064	0.978	0.033	0.815	0.291
C7	0.923	0.148	0.879	0.164	1.000	0.000	0.907	0.170	0.959	0.080	1.000	0.000	0.907	0.132	0.979	0.040	0.923	0.148
T1	0.933	0.164	0.901	0.181	1.000	0.000	0.930	0.180	0.942	0.142	1.000	0.000	0.924	0.147	0.971	0.071	0.933	0.164
T2	0.916	0.208	0.888	0.225	1.000	0.001	0.922	0.203	0.914	0.214	1.000	0.000	0.914	0.185	0.957	0.107	0.916	0.209
T3	0.889	0.264	0.863	0.272	1.000	0.000	0.881	0.284	0.881	0.264	1.000	0.000	0.886	0.244	0.948	0.121	0.876	0.284
T4	0.878	0.274	0.850	0.279	1.000	0.000	0.881	0.281	0.893	0.243	1.000	0.000	0.872	0.255	0.946	0.121	0.878	0.274
T5	0.921	0.194	0.889	0.204	1.000	0.001	0.926	0.192	0.917	0.198	1.000	0.000	0.914	0.164	0.958	0.099	0.921	0.194
T6	0.894	0.196	0.848	0.227	1.000	0.001	0.887	0.211	0.912	0.189	1.000	0.000	0.890	0.174	0.956	0.094	0.894	0.196
T7	0.885	0.227	0.843	0.255	1.000	0.000	0.864	0.268	0.867	0.268	1.000	0.000	0.884	0.205	0.947	0.112	0.860	0.267
T8	0.934	0.154	0.900	0.177	1.000	0.000	0.935	0.154	0.936	0.159	1.000	0.000	0.920	0.141	0.968	0.079	0.933	0.154
T9	0.946	0.140	0.919	0.164	1.000	0.000	0.949	0.138	0.947	0.140	1.000	0.000	0.933	0.128	0.974	0.070	0.946	0.140
T10	0.939	0.177	0.917	0.195	1.000	0.000	0.946	0.170	0.935	0.178	1.000	0.000	0.930	0.159	0.968	0.089	0.939	0.177
T11	0.945	0.166	0.923	0.180	1.000	0.000	0.952	0.153	0.941	0.171	1.000	0.000	0.936	0.140	0.971	0.085	0.945	0.166
T12	0.935	0.181	0.910	0.200	1.000	0.000	0.921	0.211	0.933	0.201	1.000	0.000	0.926	0.152	0.973	0.085	0.922	0.209
L1	0.919	0.201	0.890	0.224	1.000	0.000	0.925	0.216	0.913	0.215	1.000	0.000	0.911	0.182	0.963	0.093	0.906	0.227
L2	0.917	0.185	0.883	0.217	1.000	0.001	0.920	0.190	0.939	0.125	1.000	0.001	0.912	0.161	0.970	0.063	0.917	0.185
L3	0.939	0.161	0.912	0.186	1.000	0.001	0.943	0.165	0.943	0.155	1.000	0.001	0.925	0.154	0.971	0.078	0.939	0.161
L4	0.926	0.199	0.902	0.218	1.000	0.001	0.936	0.180	0.932	0.193	1.000	0.000	0.918	0.163	0.966	0.097	0.926	0.199
L5	0.953	0.090	0.921	0.123	1.000	0.000	0.934	0.156	0.944	0.154	1.000	0.000	0.933	0.082	0.981	0.044	0.937	0.154
Sacrum	0.968	0.035	0.940	0.054	1.000	0.000	0.961	0.055	0.977	0.011	1.000	0.000	0.931	0.043	0.989	0.006	0.968	0.035
Average	0.914		0.879		1.000		0.911		0.910		1.000		0.908		0.961		0.904	
SD	0.036		0.045		0.000		0.046		0.050		0.000		0.029		0.018		0.049	

Figure 4

A

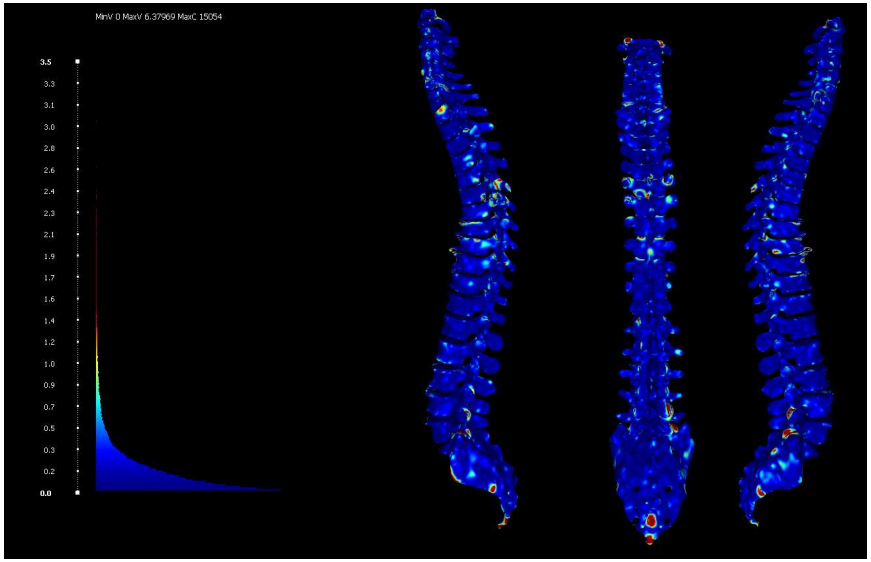

B

Metric	Hausdorff Distance (mm)		Lower 95%	Upper 9
Class	Average	SD	Confidence Interval	Confidence
C1	1.858	0.438	1.675	2.041
C2	2.028	0.428	1.845	2.211
C3	2.041	0.465	1.832	2.249
C4	2.096	0.655	1.809	2.383
C5	1.860	0.678	1.626	2.095
C6	1.854	0.508	1.716	1.993
C7	2.335	0.585	2.193	2.476
T1	2.639	0.585	2.498	2.780
T2	2.280	0.592	2.137	2.423
T3	2.675	0.766	2.491	2.858
T4	2.863	0.796	2.670	3.055
T5	2.743	0.843	2.533	2.953
T6	2.767	0.881	2.552	2.983
T7	2.687	0.865	2.484	2.890
T8	2.757	0.877	2.555	2.960
T9	2.650	0.791	2.471	2.829
T10	2.569	0.734	2.403	2.735
T11	2.643	0.775	2.471	2.815
T12	2.825	0.716	2.664	2.986
L1	2.914	0.793	2.730	3.099
L2	3.045	0.870	2.832	3.258
L3	3.263	0.789	3.060	3.466
L4	3.155	0.600	3.002	3.308
L5	2.983	0.548	2.841	3.125
Sacrum	3.566	0.572	3.415	3.717

Average	2.604
SD	0.450

C

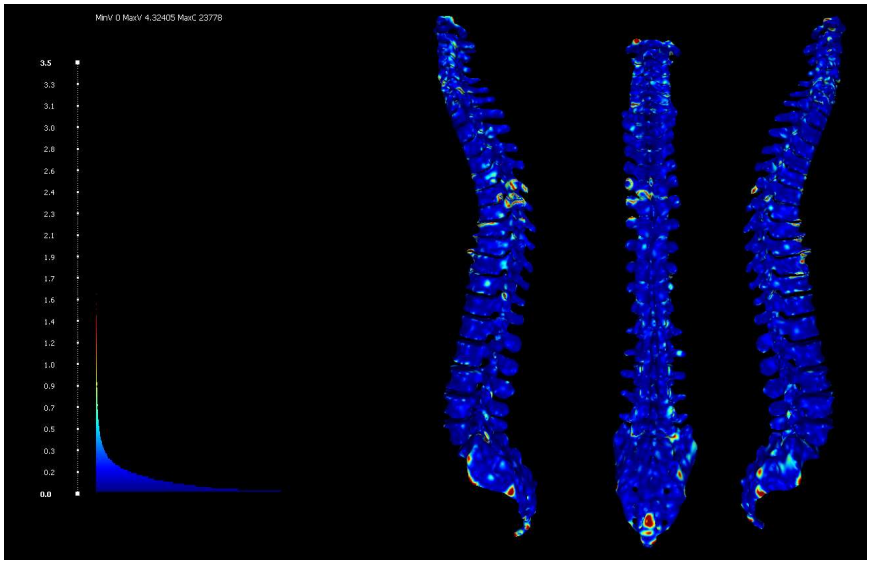

D

Metric	Hausdorff Distance (mm)		Lower 95%	Upper 9
Class	Average	SD	Confidence Interval	Confidence
C1	1.646	0.402	1.478	1.814
C2	1.753	0.474	1.550	1.955
C3	1.861	0.485	1.643	2.079
C4	1.995	0.702	1.687	2.303
C5	1.706	0.738	1.450	1.962
C6	1.609	0.472	1.481	1.737
C7	1.855	0.508	1.733	1.978
T1	2.022	0.691	1.856	2.189
T2	2.015	0.634	1.862	2.168
T3	2.130	0.652	1.974	2.286
T4	2.215	0.726	2.040	2.390
T5	2.307	0.858	2.097	2.517
T6	2.140	0.871	1.936	2.344
T7	2.173	0.927	1.959	2.387
T8	2.219	0.837	2.029	2.408
T9	2.177	0.684	2.022	2.332
T10	2.284	0.755	2.117	2.452
T11	2.475	0.811	2.293	2.658
T12	2.547	0.945	2.327	2.766
L1	2.602	1.014	2.354	2.850
L2	2.725	0.832	2.511	2.939
L3	2.642	0.800	2.438	2.846
L4	2.507	0.666	2.334	2.680
L5	3.452	0.571	3.301	3.603
Sacrum	2.287	0.816	2.084	2.490

Average	2.214
SD	0.398

Supplementary Figure 1

Metric	Dice Score			
Class	Average	SD	95% Confidence Interval Lower	95% Confidence Interval Upper
C1	0.807	0.330	0.669	0.944
C2	0.891	0.219	0.798	0.985
C3	0.891	0.211	0.796	0.985
C4	0.896	0.110	0.847	0.944
C5	0.647	0.405	0.507	0.787
C6	0.737	0.311	0.652	0.821
C7	0.812	0.222	0.758	0.866
T1	0.883	0.159	0.845	0.921
T2	0.892	0.215	0.840	0.944
T3	0.811	0.277	0.745	0.877
T4	0.804	0.282	0.736	0.872
T5	0.830	0.267	0.763	0.896
T6	0.782	0.311	0.706	0.859
T7	0.816	0.259	0.755	0.876
T8	0.879	0.195	0.834	0.924
T9	0.878	0.229	0.826	0.929
T10	0.894	0.223	0.843	0.944
T11	0.917	0.171	0.879	0.955
T12	0.915	0.166	0.878	0.953
L1	0.900	0.198	0.854	0.946
L2	0.870	0.211	0.819	0.922
L3	0.904	0.162	0.862	0.946
L4	0.883	0.211	0.829	0.937
L5	0.914	0.134	0.879	0.949
Sacrum	0.956	0.033	0.947	0.965

Average	0.856
SD	0.066

Metric	IoU			
Class	Average	SD	95% Confidence Interval Lower	95% Confidence Interval Upper
C1	0.758	0.314	0.627	0.889
C2	0.846	0.226	0.749	0.942
C3	0.840	0.207	0.746	0.933
C4	0.826	0.155	0.758	0.894
C5	0.589	0.382	0.456	0.721
C6	0.656	0.306	0.573	0.739
C7	0.724	0.225	0.670	0.779
T1	0.814	0.172	0.773	0.856
T2	0.846	0.221	0.793	0.900
T3	0.748	0.289	0.678	0.817
T4	0.739	0.295	0.668	0.810
T5	0.771	0.279	0.701	0.840
T6	0.722	0.319	0.644	0.800
T7	0.748	0.280	0.682	0.813
T8	0.819	0.214	0.770	0.869
T9	0.830	0.241	0.775	0.885
T10	0.855	0.237	0.801	0.908
T11	0.877	0.194	0.834	0.920
T12	0.872	0.190	0.829	0.915
L1	0.856	0.220	0.805	0.908
L2	0.815	0.247	0.755	0.876
L3	0.853	0.197	0.803	0.904
L4	0.833	0.230	0.774	0.892
L5	0.859	0.154	0.820	0.899
Sacrum	0.917	0.055	0.903	0.932

Average	0.801
SD	0.074

Metric	Accuracy			
Class	Average	SD	95% Confidence Interval Lower	95% Confidence Interval Upper
C1	1.000	0.000	1.000	1.000
C2	1.000	0.000	1.000	1.000
C3	1.000	0.000	1.000	1.000
C4	1.000	0.000	1.000	1.000
C5	1.000	0.000	1.000	1.000
C6	1.000	0.000	1.000	1.000
C7	1.000	0.000	1.000	1.000
T1	1.000	0.000	1.000	1.000
T2	1.000	0.001	1.000	1.000
T3	1.000	0.000	1.000	1.000
T4	1.000	0.001	1.000	1.000
T5	1.000	0.001	0.999	1.000
T6	1.000	0.001	0.999	1.000
T7	1.000	0.001	1.000	1.000
T8	1.000	0.001	1.000	1.000
T9	1.000	0.001	0.999	1.000
T10	1.000	0.001	0.999	1.000
T11	1.000	0.001	1.000	1.000
T12	1.000	0.001	1.000	1.000
L1	1.000	0.001	1.000	1.000
L2	1.000	0.001	0.999	1.000
L3	1.000	0.002	0.999	1.000
L4	1.000	0.001	0.999	1.000
L5	1.000	0.001	1.000	1.000
Sacrum	1.000	0.000	1.000	1.000

Average	1.000
SD	0.000

Metric	Precision			
Class	Average	SD	95% Confidence Interval Lower	95% Confidence Interval Upper
C1	0.796	0.327	0.651	0.941
C2	0.877	0.233	0.771	0.984
C3	0.907	0.204	0.808	1.005
C4	0.895	0.145	0.827	0.962
C5	0.668	0.423	0.516	0.820
C6	0.762	0.324	0.672	0.851
C7	0.874	0.204	0.824	0.925
T1	0.839	0.166	0.798	0.880
T2	0.905	0.212	0.853	0.957
T3	0.840	0.268	0.775	0.905
T4	0.775	0.289	0.704	0.846
T5	0.838	0.267	0.771	0.906
T6	0.783	0.310	0.706	0.860
T7	0.798	0.293	0.729	0.866
T8	0.858	0.234	0.803	0.912
T9	0.883	0.237	0.828	0.937
T10	0.911	0.217	0.862	0.961
T11	0.915	0.169	0.877	0.953
T12	0.909	0.195	0.864	0.953
L1	0.917	0.197	0.871	0.964
L2	0.920	0.189	0.873	0.968
L3	0.912	0.172	0.867	0.957
L4	0.908	0.218	0.851	0.964
L5	0.906	0.103	0.879	0.934
Sacrum	0.965	0.044	0.953	0.977

Average	0.862
SD	0.066

Metric	Sensitivity (recall)			
Class	Average	SD	95% Confidence Interval Lower	95% Confidence Interval Upper
C1	0.820	0.336	0.671	0.969
C2	0.915	0.212	0.819	1.011
C3	0.877	0.213	0.775	0.980
C4	0.911	0.090	0.869	0.953
C5	0.655	0.397	0.512	0.798
C6	0.725	0.343	0.630	0.819
C7	0.792	0.219	0.738	0.846
T1	0.945	0.146	0.909	0.981
T2	0.882	0.218	0.828	0.935
T3	0.783	0.309	0.709	0.858
T4	0.850	0.268	0.784	0.916
T5	0.826	0.270	0.758	0.895
T6	0.786	0.313	0.708	0.865
T7	0.813	0.298	0.743	0.883
T8	0.888	0.207	0.840	0.937
T9	0.877	0.221	0.826	0.927
T10	0.882	0.231	0.829	0.935
T11	0.923	0.175	0.884	0.962
T12	0.909	0.194	0.865	0.953
L1	0.906	0.175	0.865	0.948
L2	0.864	0.189	0.817	0.911
L3	0.912	0.154	0.871	0.952
L4	0.889	0.177	0.843	0.935
L5	0.936	0.137	0.900	0.972
Sacrum	0.949	0.039	0.939	0.960

Average	0.861
SD	0.070

Metric	Specificity			
Class	Average	SD	95% Confidence Interval Lower	95% Confidence Interval Upper
C1	1.000	0.000	1.000	1.000
C2	1.000	0.000	1.000	1.000
C3	1.000	0.000	1.000	1.000
C4	1.000	0.000	1.000	1.000
C5	1.000	0.000	1.000	1.000
C6	1.000	0.000	1.000	1.000
C7	1.000	0.000	1.000	1.000
T1	1.000	0.000	1.000	1.000
T2	1.000	0.000	1.000	1.000
T3	1.000	0.000	1.000	1.000
T4	1.000	0.000	1.000	1.000
T5	1.000	0.001	1.000	1.000
T6	1.000	0.000	1.000	1.000
T7	1.000	0.000	1.000	1.000
T8	1.000	0.000	1.000	1.000
T9	1.000	0.001	1.000	1.000
T10	1.000	0.001	1.000	1.000
T11	1.000	0.000	1.000	1.000
T12	1.000	0.000	1.000	1.000
L1	1.000	0.000	1.000	1.000
L2	1.000	0.000	1.000	1.000
L3	1.000	0.001	0.999	1.000
L4	1.000	0.001	1.000	1.000
L5	1.000	0.000	1.000	1.000
Sacrum	1.000	0.000	1.000	1.000

Average	1.000
SD	0.000

Metric	Boundary F1 Score			
Class	Average	SD	95% Confidence Interval Lower	95% Confidence Interval Upper
C1	0.792	0.325	0.656	0.928
C2	0.880	0.212	0.789	0.971
C3	0.894	0.134	0.833	0.954
C4	0.890	0.107	0.843	0.937
C5	0.654	0.399	0.516	0.792
C6	0.734	0.296	0.653	0.814
C7	0.783	0.196	0.736	0.830
T1	0.846	0.134	0.813	0.878
T2	0.883	0.183	0.838	0.927
T3	0.815	0.237	0.758	0.871
T4	0.787	0.251	0.726	0.847
T5	0.823	0.230	0.765	0.880
T6	0.780	0.269	0.714	0.846
T7	0.805	0.224	0.752	0.857
T8	0.850	0.173	0.810	0.890
T9	0.853	0.202	0.807	0.899
T10	0.877	0.195	0.833	0.921
T11	0.895	0.147	0.862	0.927
T12	0.885	0.152	0.851	0.919
L1	0.870	0.191	0.826	0.914
L2	0.851	0.181	0.806	0.895
L3	0.869	0.150	0.831	0.908
L4	0.846	0.188	0.798	0.894
L5	0.867	0.130	0.833	0.901
Sacrum	0.905	0.044	0.893	0.916

Average	0.837
SD	0.057

Metric	AUC			
Class	Average	SD	95% Confidence Interval Lower	95% Confidence Interval Upper
C1	0.910	0.168	0.835	0.984
C2	0.957	0.106	0.909	1.006
C3	0.939	0.107	0.887	0.990
C4	0.955	0.045	0.934	0.977
C5	0.827	0.198	0.756	0.899
C6	0.872	0.165	0.826	0.917
C7	0.896	0.110	0.869	0.923
T1	0.973	0.073	0.955	0.990
T2	0.941	0.109	0.914	0.968
T3	0.899	0.147	0.863	0.935
T4	0.925	0.134	0.892	0.958
T5	0.913	0.135	0.879	0.947
T6	0.893	0.157	0.854	0.932
T7	0.920	0.133	0.889	0.951
T8	0.951	0.089	0.930	0.972
T9	0.938	0.111	0.913	0.964
T10	0.941	0.116	0.914	0.967
T11	0.961	0.088	0.942	0.981
T12	0.961	0.081	0.943	0.979
L1	0.953	0.087	0.932	0.974
L2	0.932	0.095	0.908	0.955
L3	0.956	0.077	0.935	0.976
L4	0.944	0.088	0.921	0.967
L5	0.968	0.068	0.950	0.986
Sacrum	0.975	0.020	0.969	0.980

Average	0.932
SD	0.034

Metric	Kappa			
Class	Average	SD	95% Confidence Interval Lower	95% Confidence Interval Upper
C1	0.806	0.330	0.660	0.953
C2	0.891	0.219	0.791	0.991
C3	0.890	0.211	0.789	0.992
C4	0.896	0.110	0.844	0.948
C5	0.647	0.405	0.501	0.793
C6	0.723	0.324	0.633	0.812
C7	0.812	0.222	0.757	0.867
T1	0.883	0.159	0.844	0.922
T2	0.892	0.215	0.839	0.945
T3	0.799	0.292	0.729	0.870
T4	0.803	0.282	0.734	0.873
T5	0.830	0.267	0.762	0.897
T6	0.782	0.312	0.704	0.860
T7	0.793	0.289	0.725	0.861
T8	0.866	0.219	0.815	0.918
T9	0.878	0.229	0.825	0.930
T10	0.894	0.223	0.842	0.945
T11	0.917	0.172	0.878	0.956
T12	0.903	0.195	0.859	0.948
L1	0.900	0.198	0.853	0.947
L2	0.870	0.211	0.818	0.923
L3	0.904	0.163	0.861	0.947
L4	0.883	0.211	0.828	0.938
L5	0.914	0.134	0.878	0.949
Sacrum	0.956	0.033	0.947	0.965

Average	0.853
SD	0.068

Supplementary Figure 2

Metric	Dice Score			
Class	Average	SD	95% Confidence Interval Lower	95% Confidence Interval Upper
C1	0.843	0.303	0.716	0.970
C2	0.911	0.220	0.817	1.005
C3	0.936	0.086	0.898	0.975
C4	0.901	0.170	0.826	0.975
C5	0.794	0.271	0.700	0.888
C6	0.909	0.086	0.885	0.932
C7	0.923	0.148	0.887	0.959
T1	0.933	0.164	0.893	0.973
T2	0.916	0.208	0.866	0.967
T3	0.889	0.264	0.825	0.952
T4	0.878	0.274	0.812	0.945
T5	0.921	0.194	0.872	0.969
T6	0.894	0.196	0.846	0.943
T7	0.885	0.227	0.831	0.938
T8	0.934	0.154	0.898	0.969
T9	0.946	0.140	0.914	0.978
T10	0.939	0.177	0.899	0.979
T11	0.945	0.166	0.908	0.982
T12	0.935	0.181	0.894	0.975
L1	0.919	0.201	0.872	0.965
L2	0.917	0.185	0.872	0.962
L3	0.939	0.161	0.898	0.980
L4	0.926	0.199	0.876	0.977
L5	0.953	0.090	0.930	0.977
Sacrum	0.968	0.035	0.959	0.977

Average	0.914
SD	0.036

Metric	IoU			
Class	Average	SD	95% Confidence Interval Lower	95% Confidence Interval Upper
C1	0.805	0.308	0.677	0.933
C2	0.880	0.227	0.783	0.977
C3	0.890	0.123	0.834	0.945
C4	0.848	0.203	0.760	0.937
C5	0.720	0.287	0.620	0.820
C6	0.843	0.128	0.808	0.877
C7	0.879	0.164	0.839	0.918
T1	0.901	0.181	0.858	0.945
T2	0.888	0.225	0.834	0.942
T3	0.863	0.272	0.798	0.928
T4	0.850	0.279	0.783	0.917
T5	0.889	0.204	0.838	0.940
T6	0.848	0.227	0.792	0.903
T7	0.843	0.255	0.784	0.903
T8	0.900	0.177	0.859	0.941
T9	0.919	0.164	0.881	0.956
T10	0.917	0.195	0.873	0.962
T11	0.923	0.180	0.883	0.963
T12	0.910	0.200	0.865	0.955
L1	0.890	0.224	0.838	0.942
L2	0.883	0.217	0.829	0.936
L3	0.912	0.186	0.864	0.960
L4	0.902	0.218	0.847	0.958
L5	0.921	0.123	0.889	0.953
Sacrum	0.940	0.054	0.926	0.954

Average	0.879
SD	0.045

Metric	Accuracy			
Class	Average	SD	95% Confidence Interval Lower	95% Confidence Interval Upper
C1	1.000	0.000	1.000	1.000
C2	1.000	0.000	1.000	1.000
C3	1.000	0.000	1.000	1.000
C4	1.000	0.000	1.000	1.000
C5	1.000	0.000	1.000	1.000
C6	1.000	0.000	1.000	1.000
C7	1.000	0.000	1.000	1.000
T1	1.000	0.000	1.000	1.000
T2	1.000	0.001	1.000	1.000
T3	1.000	0.000	1.000	1.000
T4	1.000	0.000	1.000	1.000
T5	1.000	0.001	1.000	1.000
T6	1.000	0.001	1.000	1.000
T7	1.000	0.000	1.000	1.000
T8	1.000	0.000	1.000	1.000
T9	1.000	0.000	1.000	1.000
T10	1.000	0.000	1.000	1.000
T11	1.000	0.000	1.000	1.000
T12	1.000	0.000	1.000	1.000
L1	1.000	0.000	1.000	1.000
L2	1.000	0.001	1.000	1.000
L3	1.000	0.001	0.999	1.000
L4	1.000	0.001	1.000	1.000
L5	1.000	0.000	1.000	1.000
Sacrum	1.000	0.000	1.000	1.000

Average	1.000
SD	0.000

Metric	Precision			
Class	Average	SD	95% Confidence Interval Lower	95% Confidence Interval Upper
C1	0.847	0.337	1.000	1.000
C2	0.901	0.230	0.701	0.993
C3	0.970	0.025	0.796	1.005
C4	0.940	0.105	0.958	0.982
C5	0.795	0.336	0.891	0.990
C6	0.791	0.296	0.677	0.912
C7	0.907	0.170	0.713	0.869
T1	0.930	0.180	0.865	0.949
T2	0.922	0.203	0.886	0.974
T3	0.881	0.284	0.872	0.972
T4	0.881	0.281	0.812	0.949
T5	0.926	0.192	0.812	0.950
T6	0.887	0.211	0.877	0.975
T7	0.864	0.268	0.834	0.940
T8	0.935	0.154	0.800	0.927
T9	0.949	0.138	0.899	0.971
T10	0.946	0.170	0.917	0.980
T11	0.952	0.153	0.907	0.985
T12	0.921	0.211	0.918	0.987
L1	0.925	0.216	0.873	0.969
L2	0.920	0.190	0.874	0.976
L3	0.943	0.165	0.872	0.967
L4	0.936	0.180	0.899	0.986
L5	0.934	0.156	0.889	0.983
Sacrum	0.961	0.055	0.893	0.975

Average	0.911
SD	0.046

Metric	Sensitivity (recall)			
Class	Average	SD	95% Confidence Interval Lower	95% Confidence Interval Upper
C1	0.790	0.353	0.638	0.943
C2	0.928	0.213	0.831	1.025
C3	0.914	0.122	0.855	0.972
C4	0.900	0.192	0.810	0.990
C5	0.750	0.332	0.634	0.866
C6	0.852	0.299	0.774	0.931
C7	0.959	0.080	0.939	0.979
T1	0.942	0.142	0.907	0.977
T2	0.914	0.214	0.862	0.967
T3	0.881	0.264	0.817	0.945
T4	0.893	0.243	0.833	0.952
T5	0.917	0.198	0.866	0.967
T6	0.912	0.189	0.865	0.959
T7	0.867	0.268	0.804	0.930
T8	0.936	0.159	0.898	0.973
T9	0.947	0.140	0.915	0.979
T10	0.935	0.178	0.894	0.976
T11	0.941	0.171	0.903	0.980
T12	0.933	0.201	0.887	0.978
L1	0.913	0.215	0.862	0.963
L2	0.939	0.125	0.908	0.970
L3	0.943	0.155	0.902	0.984
L4	0.932	0.193	0.881	0.982
L5	0.944	0.154	0.904	0.985
Sacrum	0.977	0.011	0.974	0.980

Average	0.910
SD	0.050

Metric	Specificity			
Class	Average	SD	95% Confidence Interval Lower	95% Confidence Interval Upper
C1	1.000	0.000	1.000	1.000
C2	1.000	0.000	1.000	1.000
C3	1.000	0.000	1.000	1.000
C4	1.000	0.000	1.000	1.000
C5	1.000	0.000	1.000	1.000
C6	1.000	0.000	1.000	1.000
C7	1.000	0.000	1.000	1.000
T1	1.000	0.000	1.000	1.000
T2	1.000	0.000	1.000	1.000
T3	1.000	0.000	1.000	1.000
T4	1.000	0.000	1.000	1.000
T5	1.000	0.000	1.000	1.000
T6	1.000	0.000	1.000	1.000
T7	1.000	0.000	1.000	1.000
T8	1.000	0.000	1.000	1.000
T9	1.000	0.000	1.000	1.000
T10	1.000	0.000	1.000	1.000
T11	1.000	0.000	1.000	1.000
T12	1.000	0.000	1.000	1.000
L1	1.000	0.000	1.000	1.000
L2	1.000	0.001	1.000	1.000
L3	1.000	0.001	1.000	1.000
L4	1.000	0.000	1.000	1.000
L5	1.000	0.000	1.000	1.000
Sacrum	1.000	0.000	1.000	1.000

Average	1.000
SD	0.000

Metric	Boundary F1 Score			
Class	Average	SD	95% Confidence Interval Lower	95% Confidence Interval Upper
C1	0.838	0.296	0.714	0.962
C2	0.908	0.213	0.817	0.999
C3	0.943	0.033	0.928	0.958
C4	0.915	0.103	0.870	0.960
C5	0.822	0.250	0.735	0.908
C6	0.911	0.064	0.894	0.929
C7	0.907	0.132	0.875	0.939
T1	0.924	0.147	0.888	0.959
T2	0.914	0.185	0.869	0.959
T3	0.886	0.244	0.828	0.945
T4	0.872	0.255	0.811	0.933
T5	0.914	0.164	0.873	0.955
T6	0.890	0.174	0.847	0.932
T7	0.884	0.205	0.836	0.932
T8	0.920	0.141	0.887	0.952
T9	0.933	0.128	0.904	0.962
T10	0.930	0.159	0.894	0.966
T11	0.936	0.140	0.905	0.967
T12	0.926	0.152	0.892	0.960
L1	0.911	0.182	0.869	0.954
L2	0.912	0.161	0.873	0.952
L3	0.925	0.154	0.885	0.964
L4	0.918	0.163	0.877	0.960
L5	0.933	0.082	0.912	0.955
Sacrum	0.931	0.043	0.920	0.943

Average	0.908
SD	0.029

Metric	AUC			
Class	Average	SD	95% Confidence Interval Lower	95% Confidence Interval Upper
C1	0.917	0.155	0.850	0.984
C2	0.964	0.107	0.915	1.012
C3	0.957	0.061	0.928	0.986
C4	0.950	0.096	0.905	0.995
C5	0.904	0.138	0.856	0.952
C6	0.978	0.033	0.969	0.987
C7	0.979	0.040	0.970	0.989
T1	0.971	0.071	0.954	0.989
T2	0.957	0.107	0.931	0.983
T3	0.948	0.121	0.918	0.977
T4	0.946	0.121	0.916	0.976
T5	0.958	0.099	0.933	0.983
T6	0.956	0.094	0.932	0.980
T7	0.947	0.112	0.921	0.974
T8	0.968	0.079	0.949	0.986
T9	0.974	0.070	0.957	0.990
T10	0.968	0.089	0.947	0.988
T11	0.971	0.085	0.951	0.990
T12	0.973	0.085	0.953	0.992
L1	0.963	0.093	0.942	0.985
L2	0.970	0.063	0.954	0.985
L3	0.971	0.078	0.951	0.992
L4	0.966	0.097	0.941	0.991
L5	0.981	0.044	0.969	0.992
Sacrum	0.989	0.006	0.987	0.990

Average	0.961
SD	0.018

Metric	Kappa			
Class	Average	SD	95% Confidence Interval Lower	95% Confidence Interval Upper
C1	0.806	0.345	0.657	0.955
C2	0.911	0.220	0.811	1.011
C3	0.936	0.086	0.895	0.977
C4	0.901	0.170	0.821	0.980
C5	0.747	0.324	0.634	0.860
C6	0.815	0.291	0.738	0.891
C7	0.923	0.148	0.887	0.959
T1	0.933	0.164	0.893	0.973
T2	0.916	0.209	0.865	0.968
T3	0.876	0.284	0.807	0.944
T4	0.878	0.274	0.811	0.946
T5	0.921	0.194	0.871	0.970
T6	0.894	0.196	0.845	0.943
T7	0.860	0.267	0.797	0.923
T8	0.933	0.154	0.897	0.970
T9	0.946	0.140	0.914	0.978
T10	0.939	0.177	0.898	0.980
T11	0.945	0.166	0.907	0.982
T12	0.922	0.209	0.875	0.970
L1	0.906	0.227	0.852	0.959
L2	0.917	0.185	0.871	0.963
L3	0.939	0.161	0.896	0.981
L4	0.926	0.199	0.874	0.978
L5	0.937	0.154	0.896	0.977
Sacrum	0.968	0.035	0.959	0.977

Average	0.904
SD	0.049

Supplementary Figure 3

Metric	Dice Score			
Class	Average	SD	95% Confidence Interval Lower	95% Confidence Interval Upper
C1	0.371	0.337	0.230	0.511
C2	0.637	0.373	0.478	0.796
C3	0.578	0.333	0.428	0.727
C4	0.560	0.337	0.412	0.708
C5	0.424	0.411	0.281	0.566
C6	0.304	0.406	0.193	0.414
C7	0.285	0.406	0.187	0.383
T1	0.501	0.382	0.409	0.594
T2	0.803	0.254	0.742	0.864
T3	0.705	0.338	0.624	0.786
T4	0.598	0.405	0.500	0.696
T5	0.574	0.388	0.478	0.671
T6	0.454	0.392	0.358	0.550
T7	0.467	0.409	0.371	0.563
T8	0.548	0.385	0.459	0.637
T9	0.622	0.380	0.536	0.708
T10	0.723	0.368	0.640	0.806
T11	0.805	0.321	0.734	0.876
T12	0.791	0.315	0.721	0.862
L1	0.751	0.348	0.670	0.832
L2	0.724	0.350	0.639	0.810
L3	0.746	0.333	0.660	0.832
L4	0.743	0.331	0.659	0.827
L5	0.710	0.352	0.619	0.802
Average	0.601			
SD	0.153			

Metric	IoU			
Class	Average	SD	95% Confidence Interval Lower	95% Confidence Interval Upper
C1	0.282	0.281	0.165	0.400
C2	0.554	0.335	0.411	0.697
C3	0.471	0.298	0.337	0.606
C4	0.456	0.308	0.321	0.591
C5	0.359	0.358	0.235	0.483
C6	0.263	0.362	0.165	0.362
C7	0.252	0.368	0.163	0.341
T1	0.423	0.357	0.337	0.509
T2	0.725	0.263	0.661	0.788
T3	0.631	0.341	0.549	0.713
T4	0.536	0.387	0.442	0.629
T5	0.499	0.362	0.409	0.589
T6	0.383	0.361	0.295	0.472
T7	0.404	0.383	0.315	0.494
T8	0.471	0.364	0.387	0.555
T9	0.550	0.366	0.467	0.632
T10	0.668	0.360	0.586	0.749
T11	0.758	0.320	0.687	0.829
T12	0.738	0.327	0.665	0.812
L1	0.697	0.350	0.615	0.778
L2	0.661	0.349	0.576	0.747
L3	0.684	0.343	0.596	0.772
L4	0.678	0.341	0.591	0.765
L5	0.642	0.346	0.552	0.732
Average	0.533			
SD	0.154			

Metric	Accuracy			
Class	Average	SD	95% Confidence Interval Lower	95% Confidence Interval Upper
C1	0.999	0.001	0.999	1.000
C2	1.000	0.000	1.000	1.000
C3	1.000	0.000	0.999	1.000
C4	1.000	0.000	0.999	1.000
C5	1.000	0.000	1.000	1.000
C6	1.000	0.000	1.000	1.000
C7	1.000	0.000	1.000	1.000
T1	1.000	0.000	1.000	1.000
T2	1.000	0.001	1.000	1.000
T3	1.000	0.001	0.999	1.000
T4	1.000	0.001	1.000	1.000
T5	1.000	0.001	0.999	1.000
T6	0.999	0.001	0.999	1.000
T7	1.000	0.001	0.999	1.000
T8	1.000	0.001	0.999	1.000
T9	0.999	0.001	0.999	1.000
T10	0.999	0.001	0.999	1.000
T11	1.000	0.001	0.999	1.000
T12	1.000	0.001	0.999	1.000
L1	1.000	0.002	0.999	1.000
L2	0.999	0.002	0.999	1.000
L3	0.999	0.002	0.999	1.000
L4	0.999	0.002	0.999	1.000
L5	0.999	0.002	0.999	1.000
Average	1.000			
SD	0.000			

Metric	Precision			
Class	Average	SD	95% Confidence Interval Lower	95% Confidence Interval Upper
C1	0.660	0.463	0.455	0.865
C2	0.668	0.382	0.494	0.842
C3	0.793	0.338	0.630	0.956
C4	0.682	0.393	0.498	0.866
C5	0.423	0.412	0.275	0.572
C6	0.333	0.430	0.214	0.453
C7	0.345	0.447	0.235	0.455
T1	0.823	0.356	0.736	0.911
T2	0.822	0.254	0.760	0.884
T3	0.714	0.326	0.635	0.794
T4	0.673	0.424	0.569	0.777
T5	0.669	0.423	0.562	0.776
T6	0.579	0.444	0.468	0.690
T7	0.559	0.443	0.454	0.663
T8	0.672	0.405	0.577	0.767
T9	0.762	0.403	0.669	0.855
T10	0.774	0.386	0.685	0.863
T11	0.856	0.316	0.785	0.927
T12	0.890	0.265	0.830	0.950
L1	0.838	0.317	0.763	0.913
L2	0.814	0.334	0.731	0.898
L3	0.814	0.327	0.729	0.898
L4	0.781	0.336	0.694	0.869
L5	0.778	0.367	0.682	0.875
Average	0.697			
SD	0.150			

Metric	Sensitivity (recall)			
Class	Average	SD	95% Confidence Interval Lower	95% Confidence Interval Upper
C1	0.290	0.291	0.161	0.419
C2	0.618	0.368	0.450	0.785
C3	0.490	0.309	0.341	0.639
C4	0.488	0.312	0.342	0.634
C5	0.435	0.427	0.281	0.589
C6	0.299	0.409	0.185	0.413
C7	0.275	0.403	0.176	0.374
T1	0.439	0.368	0.348	0.529
T2	0.789	0.285	0.719	0.858
T3	0.718	0.352	0.632	0.804
T4	0.564	0.403	0.465	0.663
T5	0.527	0.373	0.433	0.622
T6	0.412	0.376	0.318	0.506
T7	0.423	0.397	0.330	0.516
T8	0.510	0.375	0.421	0.598
T9	0.562	0.370	0.477	0.647
T10	0.687	0.360	0.605	0.770
T11	0.770	0.332	0.695	0.844
T12	0.760	0.339	0.683	0.836
L1	0.735	0.348	0.653	0.818
L2	0.696	0.344	0.611	0.782
L3	0.695	0.366	0.600	0.789
L4	0.728	0.327	0.643	0.813
L5	0.660	0.361	0.565	0.755
Average	0.565			
SD	0.157			

Metric	Specificity			
Class	Average	SD	95% Confidence Interval Lower	95% Confidence Interval Upper
C1	1.000	0.000	1.000	1.000
C2	1.000	0.000	1.000	1.000
C3	1.000	0.000	1.000	1.000
C4	1.000	0.000	1.000	1.000
C5	1.000	0.000	1.000	1.000
C6	1.000	0.000	1.000	1.000
C7	1.000	0.000	1.000	1.000
T1	1.000	0.000	1.000	1.000
T2	1.000	0.000	1.000	1.000
T3	1.000	0.000	1.000	1.000
T4	1.000	0.000	1.000	1.000
T5	1.000	0.000	1.000	1.000
T6	1.000	0.000	1.000	1.000
T7	1.000	0.000	1.000	1.000
T8	1.000	0.000	1.000	1.000
T9	1.000	0.001	1.000	1.000
T10	1.000	0.001	1.000	1.000
T11	1.000	0.001	1.000	1.000
T12	1.000	0.000	1.000	1.000
L1	1.000	0.001	1.000	1.000
L2	1.000	0.000	1.000	1.000
L3	1.000	0.001	1.000	1.000
L4	1.000	0.001	0.999	1.000
L5	1.000	0.001	1.000	1.000
Average	1.000			
SD	0.000			

Metric	Boundary F1 Score			
Class	Average	SD	95% Confidence Interval Lower	95% Confidence Interval Upper
C1	0.378	0.331	0.239	0.516
C2	0.603	0.351	0.452	0.753
C3	0.588	0.307	0.450	0.726
C4	0.562	0.319	0.422	0.701
C5	0.417	0.397	0.279	0.555
C6	0.296	0.397	0.188	0.404
C7	0.278	0.394	0.183	0.373
T1	0.488	0.360	0.401	0.575
T2	0.778	0.237	0.721	0.835
T3	0.702	0.305	0.629	0.775
T4	0.600	0.372	0.511	0.690
T5	0.578	0.348	0.491	0.665
T6	0.469	0.354	0.382	0.555
T7	0.472	0.377	0.384	0.561
T8	0.535	0.355	0.453	0.617
T9	0.606	0.345	0.528	0.684
T10	0.696	0.341	0.618	0.773
T11	0.776	0.297	0.710	0.842
T12	0.772	0.285	0.708	0.835
L1	0.731	0.316	0.658	0.805
L2	0.696	0.319	0.618	0.774
L3	0.713	0.309	0.634	0.793
L4	0.712	0.301	0.635	0.788
L5	0.678	0.325	0.593	0.762
Average	0.588			
SD	0.144			

Metric	AUC			
Class	Average	SD	95% Confidence Interval Lower	95% Confidence Interval Upper
C1	0.645	0.146	0.580	0.709
C2	0.809	0.184	0.725	0.893
C3	0.745	0.154	0.671	0.819
C4	0.744	0.156	0.671	0.817
C5	0.718	0.213	0.641	0.794
C6	0.650	0.205	0.593	0.707
C7	0.637	0.201	0.588	0.687
T1	0.719	0.184	0.674	0.765
T2	0.902	0.134	0.869	0.934
T3	0.859	0.176	0.816	0.902
T4	0.782	0.201	0.732	0.831
T5	0.764	0.186	0.716	0.811
T6	0.706	0.188	0.659	0.753
T7	0.725	0.201	0.678	0.772
T8	0.755	0.188	0.711	0.799
T9	0.781	0.185	0.738	0.823
T10	0.844	0.180	0.802	0.885
T11	0.891	0.161	0.855	0.927
T12	0.886	0.164	0.849	0.923
L1	0.868	0.174	0.826	0.909
L2	0.848	0.172	0.805	0.891
L3	0.864	0.173	0.819	0.909
L4	0.864	0.164	0.821	0.906
L5	0.839	0.177	0.792	0.885
Average	0.785			
SD	0.080			

Metric	Kappa			
Class	Average	SD	95% Confidence Interval Lower	95% Confidence Interval Upper
C1	0.371	0.336	0.221	0.520
C2	0.637	0.372	0.467	0.806
C3	0.577	0.333	0.417	0.738
C4	0.560	0.337	0.402	0.718
C5	0.424	0.411	0.276	0.572
C6	0.303	0.406	0.191	0.416
C7	0.285	0.406	0.185	0.385
T1	0.501	0.382	0.408	0.595
T2	0.791	0.271	0.725	0.857
T3	0.705	0.338	0.622	0.787
T4	0.598	0.405	0.498	0.697
T5	0.574	0.388	0.476	0.673
T6	0.454	0.392	0.356	0.552
T7	0.454	0.411	0.357	0.550
T8	0.547	0.385	0.457	0.638
T9	0.622	0.380	0.534	0.709
T10	0.723	0.369	0.638	0.808
T11	0.795	0.332	0.720	0.869
T12	0.781	0.326	0.707	0.855
L1	0.751	0.348	0.669	0.833
L2	0.724	0.350	0.637	0.812
L3	0.721	0.355	0.629	0.813
L4	0.743	0.331	0.657	0.829
L5	0.698	0.362	0.603	0.793
Average	0.597			
SD	0.151			

Supplementary Figure 4

A

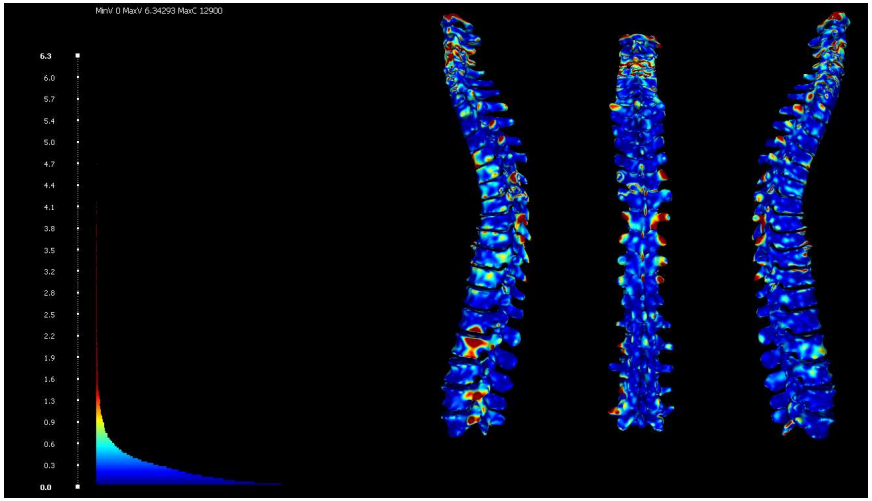

B

Metric	Hausdorff Distance (mm)		Lower 95%	Upper 95%
Class	Average	SD	Confidence Interval	Confidence Interval
C1	2.820	0.875	2.454	3.185
C2	2.965	0.647	2.688	3.242
C3	2.782	0.576	2.523	3.041
C4	2.918	0.713	2.606	3.231
C5	2.370	0.954	2.040	2.701
C6	2.482	0.652	2.305	2.659
C7	3.100	0.773	2.913	3.286
T1	3.373	0.879	3.161	3.585
T2	2.785	0.667	2.624	2.946
T3	3.032	0.844	2.830	3.234
T4	3.107	0.794	2.915	3.298
T5	3.348	0.757	3.160	3.537
T6	3.532	0.887	3.315	3.749
T7	3.479	0.946	3.258	3.701
T8	3.508	0.838	3.315	3.702
T9	3.331	0.907	3.126	3.536
T10	3.156	1.027	2.924	3.388
T11	2.972	0.919	2.768	3.176
T12	3.077	0.935	2.867	3.287
L1	3.146	0.936	2.928	3.364
L2	3.340	0.999	3.096	3.585
L3	3.622	1.092	3.341	3.903
L4	3.479	1.024	3.218	3.740
L5	3.376	0.921	3.137	3.615

Average	3.129
SD	0.322

Supplementary Figure 5

A

Metric	p-value spineCT-ResNetSeg vs spineCT_nnUNet									
Class	Dice Score	IoU	Accuracy	Precision	Sensitivity	Specificity	Boundary F1 Score	AUC	Kappa	Hausdorff Distance
C1	0.70459	0.62022	0.37299	0.60639	0.77369	0.23583	0.63048	0.88678	0.99876	0.10134
C2	0.76732	0.62264	**0.04599**	0.74846	0.84630	0.07175	0.67279	0.84609	0.76712	0.05541
C3	0.38920	0.37530	0.81518	0.19540	0.52399	0.08493	0.13669	0.52379	0.38927	0.25019
C4	0.91825	0.69562	0.70715	0.26210	0.82387	0.11134	0.45383	0.82425	0.91819	0.64195
C5	0.09377	0.12542	0.98932	0.18394	0.29629	0.24132	**0.04939**	0.07429	0.27292	0.38644
C6	**0.00029**	**0.00013**	0.55940	0.62289	**0.03974**	0.28055	**0.00009**	**0.00002**	0.11968	**0.01228**
C7	**0.00100**	**0.00002**	**0.01311**	0.32447	**0.00000**	0.70594	**0.00004**	**0.00000**	**0.00099**	**0.00000**
T1	0.07743	**0.00520**	0.29485	**0.00300**	0.90277	0.20333	**0.00176**	0.90530	0.07739	**0.00000**
T2	0.50221	0.28602	0.77267	0.63746	0.38511	0.82585	0.32729	0.38542	0.50240	**0.01414**
T3	0.09918	**0.01880**	0.43897	0.38910	0.05015	0.69282	0.08713	**0.03676**	0.12344	**0.00002**
T4	0.12399	**0.02828**	0.20584	**0.03377**	0.34078	0.21254	0.05540	0.34000	0.12387	**0.00000**
T5	**0.03212**	**0.00840**	0.33326	**0.03821**	**0.03608**	0.29437	**0.01227**	**0.03611**	**0.03218**	**0.00273**
T6	**0.01649**	**0.01140**	0.37949	**0.02841**	**0.00710**	0.48161	**0.00721**	**0.00712**	**0.01653**	**0.00330**
T7	0.09539	**0.03637**	0.30951	0.16098	0.25788	0.11183	**0.03190**	0.19187	0.14948	**0.00028**
T8	0.06248	**0.01513**	0.12454	**0.01994**	0.12454	0.08958	**0.00857**	0.23178	**0.03474**	**0.00016**
T9	**0.02940**	**0.00959**	0.13170	**0.03971**	**0.02133**	0.15602	**0.00441**	**0.02125**	**0.02933**	**0.00145**
T10	0.16943	0.07827	0.17091	0.27567	0.11463	0.24472	0.06896	0.11449	0.16902	**0.00091**
T11	0.30885	0.12574	0.33137	0.14648	0.50813	0.30453	0.07663	0.50723	0.30843	**0.00396**
T12	0.49914	0.23033	0.52564	0.69929	0.46163	0.98056	0.09686	0.38318	0.56405	**0.00552**
L1	0.57887	0.36898	0.78695	0.82605	0.83668	0.95313	0.18787	0.49408	0.86899	**0.01320**
L2	0.18699	0.10461	0.68086	0.98805	**0.00890**	0.76718	**0.04443**	**0.00897**	0.18701	**0.00902**
L3	0.24919	0.10319	0.47364	0.32719	0.27620	0.44883	0.05272	0.27548	0.24888	**0.00051**
L4	0.25326	0.09455	0.45636	0.43427	0.20754	0.33812	**0.02724**	0.20696	0.25294	**0.00015**
L5	0.06874	**0.02030**	0.44177	0.25953	0.76385	0.17086	**0.00164**	0.24012	0.39430	**0.00006**
Sacrum	0.06283	**0.03119**	0.15076	0.69608	**0.00000**	0.64117	**0.00198**	**0.00000**	0.06199	0.29829

B

Metric	p-value spineCT-ResNetSeg vs MONAI-Verse									
Class	Dice Score	IoU	Accuracy	Precision	Sensitivity	Specificity	Boundary F1 Score	AUC	Kappa	Hausdorff Distance
C1	**0.00009**	**0.00000**	**0.00999**	0.26757	**0.00000**	**0.04576**	**0.00014**	**0.00000**	**0.00009**	**0.00007**
C2	**0.01107**	**0.00219**	**0.00194**	**0.03920**	**0.00309**	**0.03918**	**0.00393**	**0.00304**	**0.01103**	**0.00000**
C3	**0.00162**	**0.00011**	**0.00301**	0.21819	**0.00011**	0.77313	**0.00054**	**0.00008**	**0.00162**	**0.00011**
C4	**0.00031**	**0.00005**	**0.00841**	**0.03238**	**0.00001**	0.29519	**0.00022**	**0.00001**	**0.00031**	**0.00051**
C5	**0.03262**	**0.01585**	**0.04449**	**0.02216**	**0.03347**	**0.01699**	**0.02030**	**0.03712**	**0.03256**	**0.01675**
C6	**0.00000**	**0.00000**	**0.01378**	**0.00000**	**0.00000**	0.28034	**0.00000**	**0.00000**	**0.00000**	**0.00000**
C7	**0.00000**	**0.00000**	**0.00285**	**0.00000**	**0.00000**	0.64321	**0.00000**	**0.00000**	**0.00000**	**0.00000**
T1	**0.00000**	**0.00000**	**0.04222**	0.75315	**0.00000**	**0.04798**	**0.00000**	**0.00000**	**0.00000**	**0.00000**
T2	**0.03197**	**0.00472**	0.49916	**0.04358**	**0.03495**	0.60738	**0.00550**	0.06750	**0.01881**	**0.00001**
T3	**0.04869**	**0.03442**	0.10117	**0.01611**	0.26632	0.06077	**0.01845**	0.15439	0.08519	**0.01131**
T4	**0.00098**	**0.00093**	0.17255	0.10940	**0.00001**	0.41258	**0.00100**	**0.00000**	**0.00098**	0.08011
T5	**0.00004**	**0.00001**	0.33749	**0.00890**	**0.00000**	0.70684	**0.00001**	**0.00000**	**0.00004**	**0.00005**
T6	**0.00000**	**0.00000**	0.16731	**0.00313**	**0.00000**	0.68572	**0.00000**	**0.00000**	**0.00000**	**0.00000**
T7	**0.00000**	**0.00000**	0.16460	**0.00021**	**0.00000**	0.97582	**0.00000**	**0.00000**	**0.00000**	**0.00000**
T8	**0.00000**	**0.00000**	0.11214	**0.00102**	**0.00000**	0.96214	**0.00000**	**0.00000**	**0.00000**	**0.00000**
T9	**0.00000**	**0.00000**	0.25478	**0.02706**	**0.00000**	0.87060	**0.00000**	**0.00000**	**0.00000**	**0.00000**
T10	**0.00080**	**0.00026**	0.35119	**0.00841**	**0.00013**	0.78478	**0.00011**	**0.00014**	**0.00081**	**0.00009**
T11	**0.00752**	**0.00576**	0.36233	0.14362	**0.00040**	0.65906	**0.00195**	**0.00084**	**0.00414**	**0.01684**
T12	**0.00295**	**0.00248**	0.14787	0.62042	**0.00101**	0.94077	**0.00269**	**0.00051**	**0.00541**	0.06433
L1	**0.00221**	**0.00150**	0.22585	0.07469	**0.00034**	0.44340	**0.00194**	**0.00035**	**0.00220**	0.11389
L2	**0.00509**	**0.00474**	0.46612	**0.02918**	**0.00089**	0.52267	**0.00107**	**0.00095**	**0.00511**	0.07658
L3	**0.00171**	**0.00157**	0.57122	**0.04284**	**0.00006**	0.74193	**0.00083**	**0.00033**	**0.00051**	**0.04490**
L4	**0.00731**	**0.00483**	0.35114	**0.01723**	**0.00127**	0.41694	**0.00448**	**0.00130**	**0.00731**	**0.03846**
L5	**0.00012**	**0.00004**	0.11469	**0.01287**	**0.00000**	0.27333	**0.00011**	**0.00000**	**0.00006**	**0.00686**